

## Response of the bottom boundary layer over a sloping shelf to variations in alongshore wind

A. Perlin, J. N. Moum, and J. M. Klymak<sup>1</sup>

College of Oceanic and Atmospheric Sciences, Oregon State University, Corvallis, Oregon, USA

Received 20 May 2004; revised 22 October 2004; accepted 30 December 2004; published 14 September 2005.

[1] Rapidly repeated transects of currents, density, and turbulence through the bottom boundary layer across a relatively uniform stretch of the continental shelf off Oregon reveal the response to a sequence of strong upwelling followed by relaxation and thence a resumption of upwelling. Several definitions of boundary layer thickness are employed to describe the evolution of the bottom boundary layer. Well-mixed and turbulent layers were typically confined to 10 m from the bottom. However, boundary layer thicknesses were greatest during relaxation from upwelling (when mixed layer and turbulent layer thicknesses exceeded 20 m), and turbulence in the bottom boundary layer was most intense at this time. Dense, near-bottom fluid was observed to move upslope with upwelling and back down the slope with relaxation from upwelling. By tracking the intersection of near-bottom isopycnals with the bottom over successive transects, we estimate the cross-shore speed of fluid in the bottom boundary layer. Cross-shore speed agrees well with dynamical estimates of cross-shore velocity in the bottom Ekman layer derived from bottom stress measurements. This leads to a confirmation of the Ekman balance of alongshore momentum in the bottom boundary layer across the full width of the shelf. Good correlation exists between alongshore velocity at the top of the bottom boundary layer and cross-shore velocity of dense fluid in the bottom boundary layer. Application of a derived proxy for bottom stress to moored velocity observations indicates Ekman balance of alongshore momentum at a midshelf location (81 m depth) for a 3 month period in spring/summer 2001.

**Citation:** Perlin, A., J. N. Moum, and J. M. Klymak (2005), Response of the bottom boundary layer over a sloping shelf to variations in alongshore wind, *J. Geophys. Res.*, 110, C10S09, doi:10.1029/2004JC002500.

### 1. Introduction

[2] Cross-shelf circulation in coastal upwelling regions is determined to a great extent by flows in the surface and bottom boundary layers (BBL). Wind forcing generates cross-shore motion of water in the surface Ekman layer. This, in turn, creates a pressure gradient which drives alongshore flow beneath the surface layer. A consequence of this alongshore flow is a near-bottom Ekman transport opposite in direction to that in the surface layer.

[3] It has proven to be quite difficult to obtain clear observations of cross-shore motion in the BBL. Moored velocity measurements in the BBL have indicated the complexity of the temporal structure of the BBL [Weatherly, 1972; Mercado and van Leer, 1976; Kundu, 1976; Dickey and van Leer, 1984; Saylor and Miller, 1988; Saylor, 1994; Lass and Mohrholz, 2003; Perlin et al., 2005a]. Only recently has there been the combination of measurements necessary for a direct observational test of Ekman dynamics in the BBL [Trowbridge and Lentz, 1998]. From finely

resolved velocity profiles through the BBL and near-bottom turbulence stress measurements of sufficiently long duration that superinertial fluctuations could be filtered out, Trowbridge and Lentz [1998] clearly showed the dominant balance between Coriolis force and turbulence stress divergence in the alongshore momentum equation at a location on the California coast.

[4] The Ekman balance of alongshore momentum in the BBL can be rephrased to state that the cross-shore fluid transport within the BBL can be estimated from a local measurement of bottom stress. In the case that alongshore variations of fluid properties in the BBL and vertical mixing are relatively small, the cross-shore transport can be estimated by tracking the cross-shore motion of a representative fluid property. This can be compared to local bottom stress measurements to test the balance. Such an analysis represents a test of the Ekman balance of alongshore momentum across the entire width of the shelf. In the spring of 2001, we had the opportunity to rapidly repeat transects across the continental shelf over a period of 8 days that included two upwelling/relaxation cycles. Detailed observations of the density structure and turbulence were made to within 2 cm of the bottom. From these observations, a detailed view of the vertical and cross-shore structure of the BBL was obtained. Using the density to track fluid transport in the

<sup>1</sup>Now at Scripps Institution of Oceanography, University of California, San Diego, La Jolla, California, USA.

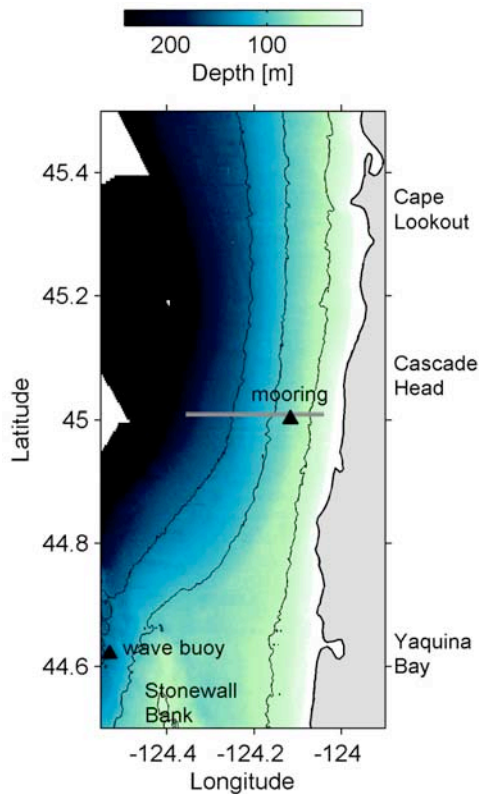


**Figure 1.** Bathymetry of the central Oregon coast. The dark line indicates the location of 12 transects made over the period 19–28 May 2001. Locations of the Stonewall Bank wave buoy and mooring are noted.

BBL and an estimate of bottom stress from our turbulence measurements, we test the alongshore momentum balance in the BBL.

[5] The observational site and overview of the data are presented in the next two sections, followed by a description of both the vertical and cross-shelf structure of the BBL. We then estimate (both kinematically and dynamically) the cross-shelf motion of near-bottom fluid in the BBL in response to variations in alongshore current. This is followed by an extended test of the Ekman balance in the BBL over a 3 month period using moored observations. Other contributions to the alongshore momentum are considered in the discussion.

## 2. Experimental Details

[6] Our observations were made in late spring 2001 from the R/V *Thomas G. Thompson* as part of a larger field experiment (Coastal Ocean Advances in Shelf Transport (COAST)). During this experiment, twelve detailed transects were repeated over a period of 8 days across a line directly offshore (west) from Cascade Head ( $45^{\circ}0'30''$ ). The transects extended from the 30 m depth contour to the shelf break at about 190 m depth (25 km offshore (Figure 1)).

[7] Velocity data were collected using 150 kHz shipboard acoustic Doppler current profiler (ADCP), sampled at 5 s and 4 m depth bins, and subsequently averaged over 3 min. Good velocity data is in the range from 20 m below the surface to about 85% of the water depth. Wind data from

shipboard sensors as well as winds from the Stonewall Bank wave buoy (NDBC buoy 46050 (Figure 1)) were used for computations of wind stress. The wave buoy data are used here to describe the wind history in the days prior to our arrival at the observation site. Ship winds are used for all other purposes.

[8] Vertical profiles were made using our loosely tethered turbulence profiler, Chameleon. Deployed with a bottom crusher to prevent probe damage in collisions with the bottom, we routinely profiled Chameleon into the bottom, permitting profiles to within 2 cm of the seabed. Chameleon has sensors to measure pressure, acceleration, temperature, conductivity, turbidity (880 nm backscatter), and microstructure shear (using airfoil probes). A detailed description of Chameleon and how the data is processed to estimate the turbulent kinetic energy dissipation rate,  $\epsilon$ , from velocity microstructure shear can be found in the work of *Moum et al.* [1995].

[9] Our typical mode of operation was to cross the shelf from the inshore side. Because we operated simultaneously with a continuously profiling pumped system, the ship was oriented so as to prevent crossing of the two wires. This typically required pointing the ship into the wind or current. With prevailing northerlies and a southward surface current, we crabbed across the shelf, moving west while heading west of north. Cross-shelf transit speeds were in the range 1–1.5 kts. At our mean profiling speed of  $1 \text{ m s}^{-1}$ , we made profiles at less than 2 min intervals inshore (75 m horizontal separation) and about 6 min intervals offshore ( $200^+$  m horizontal separation). While in situ profiling measurements were only made while moving offshore, continuous ADCP measurements provided snapshots of the velocity field as we repositioned to our inshore starting point (at 10 kts).

## 3. Overview

[10] A record of wind stress from the period 6 days preceding and during our measurements is shown in Figure 2 (NOAA wave buoy data is used here to show wind stress). Strong, southerly (downwelling-favorable) winds prior to our arrival yielded to northerlies (upwelling-favorable) by the time we began our observations on 19 May. Winds remained northerly for 3.5 days, slackening and turning to weak southerly for 2 days before returning again to moderate upwelling-favorable winds for 2.5 days and again slackening. This timely sequence permitted us the opportunity to obtain detailed observations of the cross-shore structure of velocity, density, and turbulence through one complete and one partial upwelling-relaxation cycle. We have assigned a time base of hours relative to the beginning of our observations to each transect to guide in the description of the time sequence of events. This is noted at the top of Figure 2.

[11] Upwelling-favorable winds had been developing and building 2 days prior to the beginning of our observations (Figure 2, from the Yaquina Bay wave buoy). By the time of our first transect (0 hours), a strong southward surface current extended across the shelf (Figure 3). The surface current subsequently strengthened and shifted offshore (+24 hours) and back onshore (+64 hours). Superimposed on the wind-driven currents were tidal currents that are spatially and temporally aliased by our sampling scheme. Moored records [*Boyd et al.*, 2002] indicate that the cross-

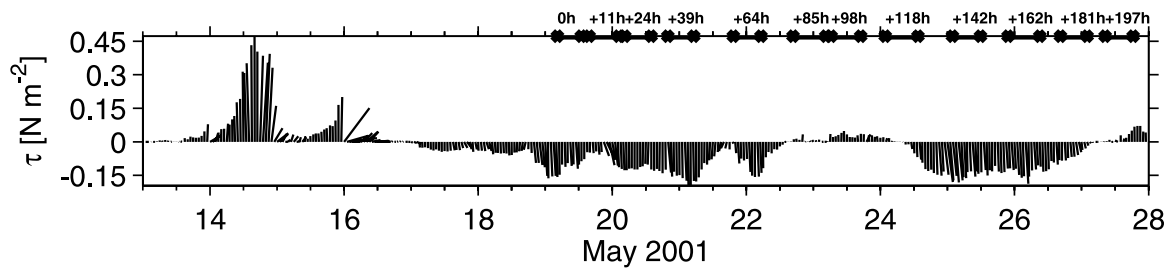


**Figure 2.** Wind stress computed with data obtained from the wave buoy at station 46050 (Stonewall Bank, Figure 1). The times of the 12 transects are marked along the top of the box. Times (in hours) are relative to the beginning of the first transect.

shore component of the flow is highly baroclinic, of magnitude  $0.1 \text{ m s}^{-1}$  and predominantly tidal. Once upwelling winds had weakened (+85 hours) the surface current relaxed and a northward-flowing undercurrent appeared offshore of 20 km, extending across the shelf between +85 hours and +98 hours, appearing only inshore at +98 hours and +118 hours. With the resumption of upwelling winds, the southward surface current reestablished itself.

[12] An important aspect of the variations in the cross-shelf structure of the density during this progression of states from upwelling to relaxation and back to upwelling is the upslope advance and downslope retreat of the near-bottom fluid. This is illustrated in Figure 3 by the thick near-bottom isopycnal ( $\sigma_\theta = 26.6$ ;  $\sigma_\theta$  is potential density). The intersection of this isopycnal with the bottom marks the shoreward extent of near-bottom fluid with  $\sigma_\theta \geq 26.6$ . This dense, near-bottom fluid advances upslope during upwelling (at both the beginning and the end of our observation period) and retreats back down the slope with the cessation of upwelling winds.

[13] Turbulence (as indicated by  $\epsilon$  in Figure 3) is high near the bottom, inshore and, more intermittently, in the interior. The location of high BBL turbulence varies across the shelf. Generally (but not always), high near-bottom turbulence is associated with high near-bottom currents. The integrated dissipation rate (vertical and cross-shelf) is shown in the bar plots inset in the  $\epsilon$  image plots; the highlighted bar represents the current transect. To exclude the influence of ship wake on turbulence, the surface 20 m are not included in the integration. The integrated dissipation rate is high in transects +24 hours and +39 hours, when the alongshore flow is strongest and shear in the BBL is highest (as reflected by high alongshore velocities in the lowest ADCP bin). By the end of the upwelling cycle, and with the weakening of southward currents, near-bottom shear weakened and near-bottom turbulence decreased. With the resumption of downwelling-favorable winds, near-bottom waters retreated offshore, accompanied by

reduced near-bottom stratification. During this phase, the BBL was thickest and turbulence was high in the absence of strong near-bottom currents and strong shear (discussed further in section 4). Integrated turbulence was highest during this phase (+98 hours). During relaxation, integrated turbulence was high due to the intense turbulence in the BBL, and also due to strong inshore turbulence in the vicinity of the northward subsurface flow. With resumption of upwelling-favorable winds, the southward jet was reestablished. Near-bottom water began moving up the slope once again, increasing near-bottom stratification. At this point, the jet was still weak and near-bottom shear was low, and turbulence decreased to its lowest values both in the BBL and integrated across the transect.

[14] Our optical backscatter sensor (880 nm) is relatively insensitive to particles much larger than its wavelength (because they do not occur very often in the light path; particles on the scale of the viscous sublayer appear as occasional spikes in the data). The turbidity in the water column is high near the bottom and inshore. Near the bottom, regions of high turbidity are usually associated with regions of high turbulence (as demonstrated in Figure 4). Inshore, the highest turbidity occurred coincident with intense inshore turbulence, suggesting that turbulence was responsible for resuspension of fine material. Turbidity was also high along thin tendrils that lie on isopycnals and extend continuously from inshore to 20<sup>+</sup> km offshore. These tendrils are continuous inshore to water depths less than 30 m.

#### 4. Structure and Properties of the Bottom Boundary Layer (BBL)

[15] Our perspective of the BBL comes from finely resolved vertical profiles to within 2 cm of the bottom. Example profiles are shown in Figure 5. The typical structure shows energetic and intermittent velocity turbulence increasing toward the bottom as in the second panel of Figure 5a. This is loosely constrained by the height of the

**Figure 3.** (left) Alongshore currents ( $v$ ), (middle) turbulent dissipation rate ( $\epsilon$ ), and (right) turbidity (880 nm optical backscatter) from an 8 day period beginning 19 May 2001, during which 12 transects were made across the shelf off Cascade Head. Isopycnals are plotted over each image, and the 26.6 isopycnal is highlighted as an indicator of cross-shelf motion of dense near-bottom fluid. Relative wind stress averaged over the 24 hour period preceding each transect is shown to the right (upwelling-favorable downward). The relative time of each transect is shown in the leftmost column, starting with 0 hours at the beginning of the first transect. In the lower right-hand corner of the  $\epsilon$  image plot is shown the transect-averaged dissipation (units of  $\text{W per m}$  of alongshore distance linearly scaled such that  $200 \text{ W m}^{-1}$  corresponds to  $100 \text{ m}$  on depth scale and 0 to the bottom of the plot); the highlighted bar represents the current transect. Locations of the example profiles from Figure 5 are marked on the panels in red.

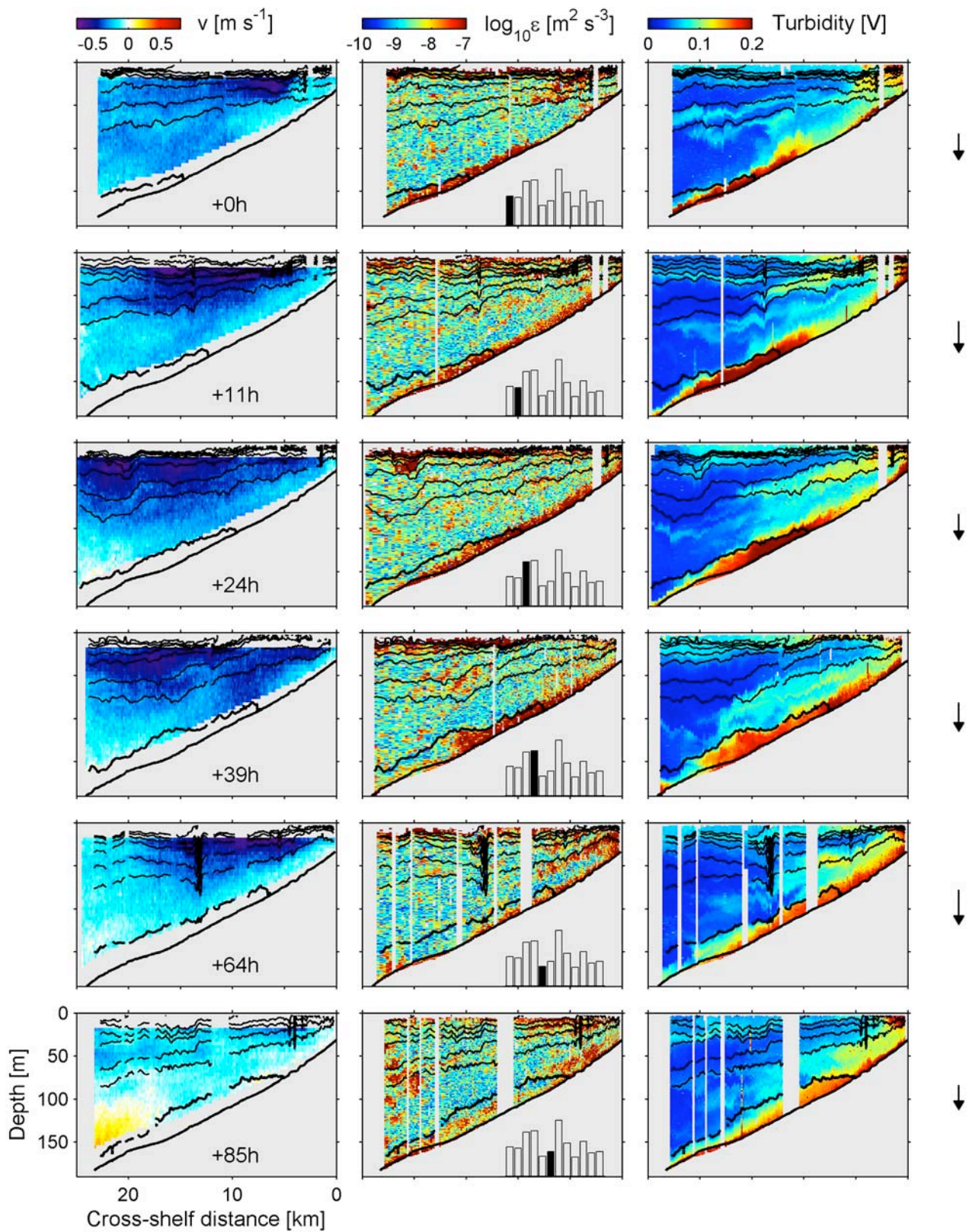


Figure 3

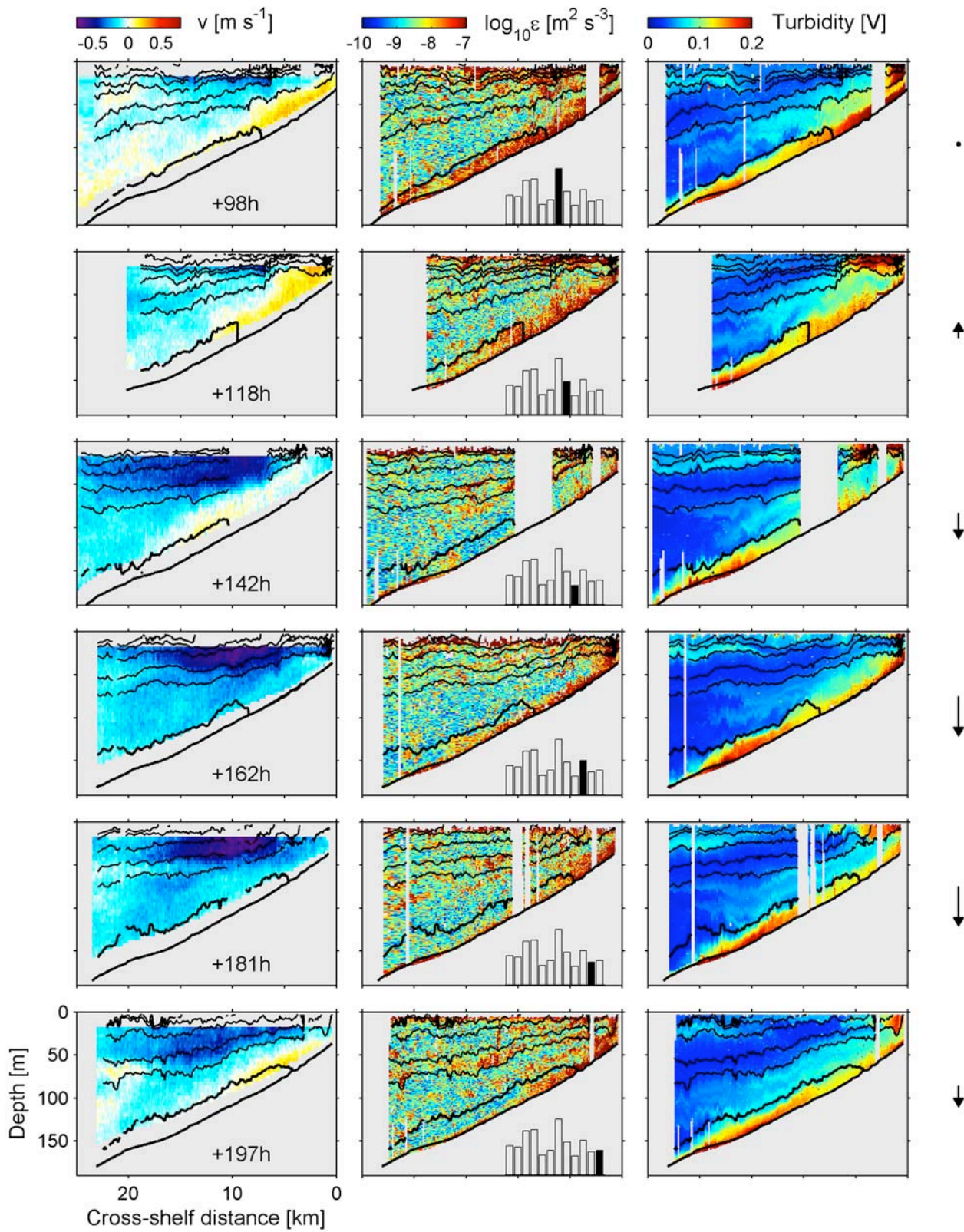
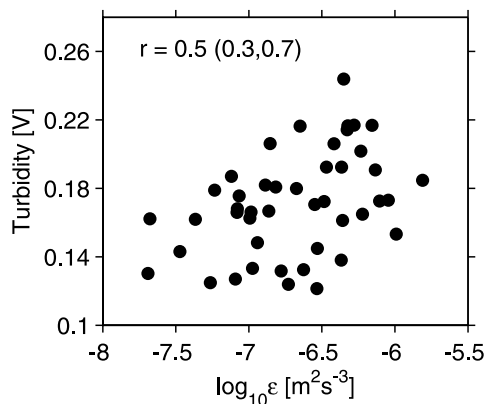


Figure 3. (continued)



**Figure 4.** Bottom boundary layer (BBL) turbidity versus  $\varepsilon$ . These averages were made over 5 km cross-shelf ranges in the bottom mixed layer. The correlation coefficient with 95% confidence limits is shown at the top of the plots.

mixed layer near the bottom. Any definition of a mixed layer is not straightforward and these four example profiles indicate the variations in vertical structure of density as well as the observed variations in different definitions of BBL thickness. Stratification is weakest at and near the bottom where turbulence is most energetic. For our analysis we term this the bottom mixed layer (denoted by  $D$ ) and define it objectively as the distance from the bottom over which  $\sigma_\theta$  decreased by  $6 \times 10^{-4} \text{ kg m}^{-3}$  from its bottom value (the bottom value is defined as the mean value of the five bottommost data points, representing the bottom 10 cm). The value  $6 \times 10^{-4} \text{ kg m}^{-3}$  is sufficiently large compared to the precision of our density estimate yet small enough to clearly define  $D$  based on visual comparison to hundreds of individual profiles. To avoid the effects of local overturns in the estimation of  $D$ , we then required that  $\sigma_\theta$  remain below this value for 50 consecutive data points 1 m above  $D$ . Above the mixed layer there is typically a weakly stratified layer, which we term the remnant layer ( $D_r$ ), defined as the distance from the bottom over which  $\sigma_\theta$  decreases by  $0.03 \text{ kg m}^{-3}$ . The remnant layer is usually capped by a strongly stratified layer, as seen in the four example profiles in Figure 5. The turbulent bottom layer ( $D_\varepsilon$ ) is defined as the depth below which  $\varepsilon$  remained above  $6 \times 10^{-9} \text{ m}^2 \text{ s}^{-3}$ . Turbulence in the BBL decreases from high values near the bottom to lower levels in the interior above. The threshold for the automatic selection of  $D_\varepsilon$  was chosen empirically, based on an evaluation of several hundred profiles. Each of these layer definitions is arbitrary to a certain extent. However, taken together they provide an aid to understanding the cross-shelf structure and evolution of the BBL.

[16] The four example profiles shown in Figure 5 are intended to demonstrate the range of variations in layer heights. Locations of the example profiles are marked in Figures 3 and 6. Figure 5a shows the thick turbulent layer at a time when near-bottom shear is high (see Figure 3). Figures 5b and 5c are representative of downwelling conditions in which thick mixed layers and weakly stratified remnant layers are accompanied by thick turbulent layers. Figure 5b demonstrates an example in which the turbulent layer is thicker than the mixed layer, and Figure 5c is an example where the well-mixed layer is as thick as the

turbulent layer. Low near-bottom velocities at the beginning of the upwelling cycle correspond to the profile shown in Figure 5d: thin turbulent and mixed layers. At this stage, the thick remnant layer is likely a remnant of the downwelling conditions preceding this transect. This variability demonstrates that mixed and turbulent boundary layers do not necessarily coincide with each other.

[17] Another relevant length scale in the BBL is the thickness over which bottom friction acts to effect a rotation of the current vector, leading to transport perpendicular to that in the interior; this defines the bottom Ekman layer. Our shipboard ADCP velocity measurements are insufficiently close to the bottom to estimate the veering layer height. They are also insufficiently long to filter out non-Ekman velocity fluctuations. *Perlin et al.* [2005b] use near-bottom moored velocity data to show that  $D_\varepsilon$  is a relatively good indicator of bottom Ekman layer thickness.

[18] The cross-shore distribution and temporal evolution of BBL heights is shown in Figure 6. In that figure,  $D$  ranges from  $<5$  to  $>20$  m,  $D_r$  ranges from  $<5$  to  $>30$  m, and  $D_\varepsilon$  ranges from  $<5$  to 20 m. A systematic variation in layer heights is evident. Our sequence of transects includes a period of sustained upwelling during which dense fluid is drawn up the shelf. As winds decreased and turned to the north (+98 hours), dense fluid in the BBL moved down the slope. Coincidentally, both  $D$  and  $D_\varepsilon$  increased (+118 hours). Following reversal of winds to the south,  $D$  and  $D_\varepsilon$  decreased, while  $D_r$  remained large across the shelf. Hence the term “remnant layer” is a reference to the thick, moderately mixed layer, which remains after active mixing has ceased. While the largest values of near-bottom shear occur during upwelling, the BBL is thickest (by all of its kinematic measures, i.e., mixed and turbulent layers) following the weakening of upwelling-favorable winds. This indicates the asymmetry in response to upwelling/relaxation in the behavior of the BBL observed by *Trowbridge and Lentz* [1991]. During this period, *Moum et al.* [2004] have demonstrated the existence of convectively driven mixing in the BBL which they have attributed to the offshore transport of light fluid beneath dense fluid due to the near-bottom maximum in the cross-shore Ekman velocity profile.

[19] Figure 6 shows the variability of layer heights in the cross-shelf direction. It is evident that the variability is greatest in the midshelf region. On average, it is also thicker at midshelf than either inshore or offshore. In contrast to the findings of *Lentz and Trowbridge* [1991], no general increase in BBL thickness with depth was observed.

[20] The water mass characteristics of the BBL remained relatively constant during our 8 day observation period. This is seen in the constancy of  $\theta S$  properties (Figure 7). The data shown in Figure 7 represent averaged values of  $\theta$  and  $S$  over  $D$  from individual profiles, with the initial transect color coded to represent cross-shelf location. While  $\sigma_\theta$  did not always increase monotonically offshore in the BBL, the distribution of  $\theta S$  was relatively consistent across the shelf for all of the 12 transects.

## 5. Cross-Shelf Motion of Dense Fluid in the BBL

### 5.1. Theory

[21] In a rotating fluid, boundary stress on a current drives a near-boundary transport transverse to the current.

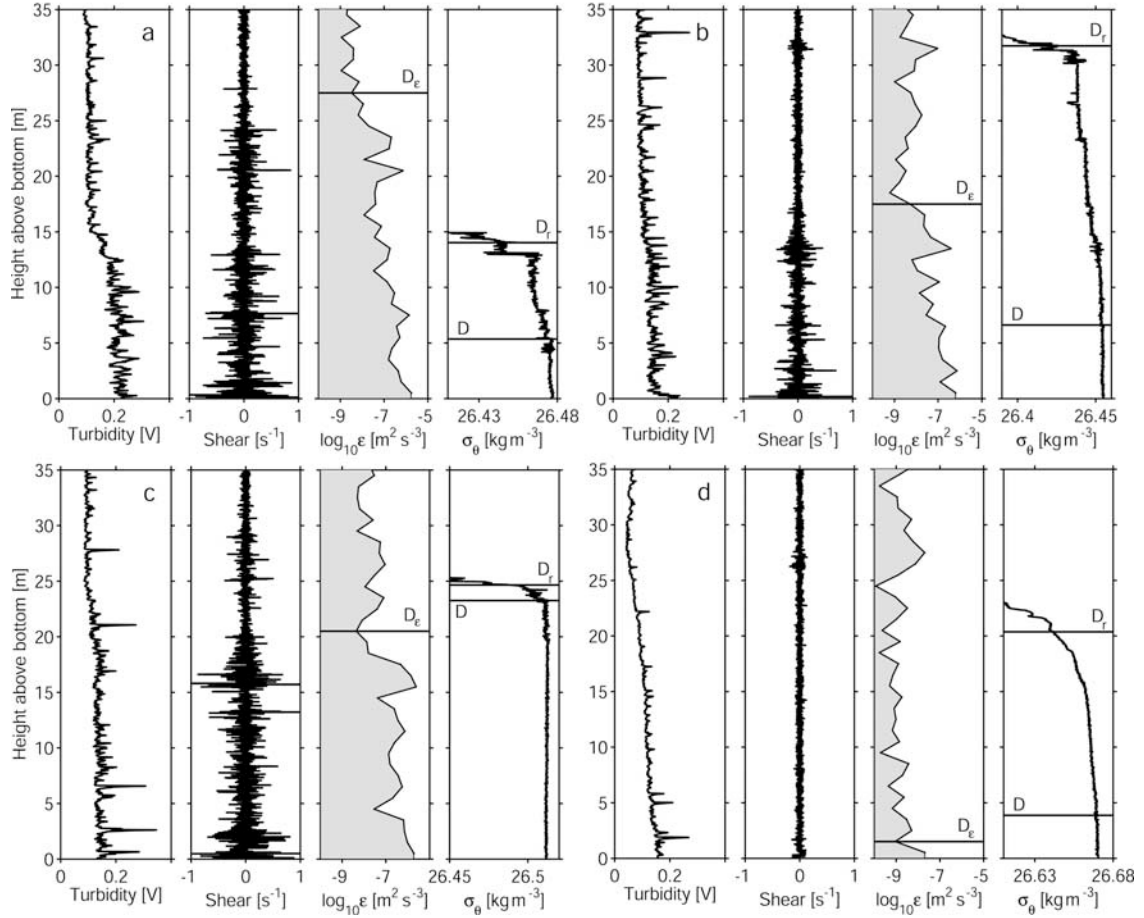


**Figure 5.** Individual Chameleon profiles showing different aspects of the vertical structure of the BBL. Shown here are turbidity sensed by an 880 nm backscatter sensor mounted on Chameleon’s nose, microscale velocity shear, turbulent dissipation rate ( $\epsilon$ ), and  $\sigma_\theta$ . The horizontal line in the third panel of each plot is an indication of the turbulent boundary layer height ( $D_\epsilon$ ). In the rightmost column are shown the heights of mixed layer ( $D$ ) and remnant layers ( $D_r$ ) as determined objectively from density profiles. In Figure 5a the turbulent layer is above the remnant layer, in Figure 5b it is in the remnant layer, in Figure 5c it is at the top of the mixed layer (which is approximately collocated with the remnant layer), and in Figure 5d it is contained within a shallow mixed layer.

This is the basis of Ekman theory. At an eastern boundary, bottom stress on the southward current formed by the coastal upwelling circulation drives a bottom Ekman layer up the sloping shelf toward the shore. The dynamics of the boundary layer are described by simplified momentum and density equations for a Boussinesq fluid [e.g., Pedlosky, 1987]. The alongshore ( $y$  coordinate direction) momentum equation reduces to

$$\rho_0 \frac{\partial v}{\partial t} + \rho_0 f u = -\frac{\partial p}{\partial y} + \frac{\partial \tau_y}{\partial z}. \quad (1)$$

The density equation reduces to

$$\frac{\partial \rho}{\partial t} + u \frac{\partial \rho}{\partial x} + v \frac{\partial \rho}{\partial y} = \frac{\rho_0}{g} \frac{\partial J_b}{\partial z}. \quad (2)$$

Here  $g$  is gravitational acceleration;  $f$  is the Coriolis parameter;  $(u, v)$  is the velocity vector;  $p$  is pressure;  $\tau_y$  is the stress component in the  $y$  component direction;  $\rho$  is density;  $\rho_0$  is background density; and  $J_b = -(g/\rho_0)\rho'w'$ ,

which also can be written as  $J_b = -(g/\rho_0)K_\rho(\partial\rho/\partial z)$ , where the latter represents the definition of the turbulent diffusion coefficient,  $K_\rho$ , and  $g$  is acceleration of gravity.

[22] For steady state flow and zero alongshore pressure gradient, (1) reduces to a classical Ekman balance:

$$f u = \frac{1}{\rho_0} \frac{\partial \tau_y}{\partial z}. \quad (3)$$

Assuming that the shear stress atop the Ekman layer is much smaller than the bottom stress, vertical integration of (3) over an Ekman layer of thickness  $D_{Ek}$  yields the mean cross-shore Ekman transport,  $\vartheta_{Ek}$ , in terms of bottom stress:

$$\vartheta_{Ek} = \frac{\tau_{yb}}{\rho_0 f}. \quad (4)$$

From this is derived the vertically averaged cross-shore Ekman velocity over  $D_{Ek}$ :

$$u_{Ek} = \frac{\vartheta_{Ek}}{D_{Ek}} = \frac{\tau_{yb}}{\rho_0 D_{Ek} f}. \quad (5)$$

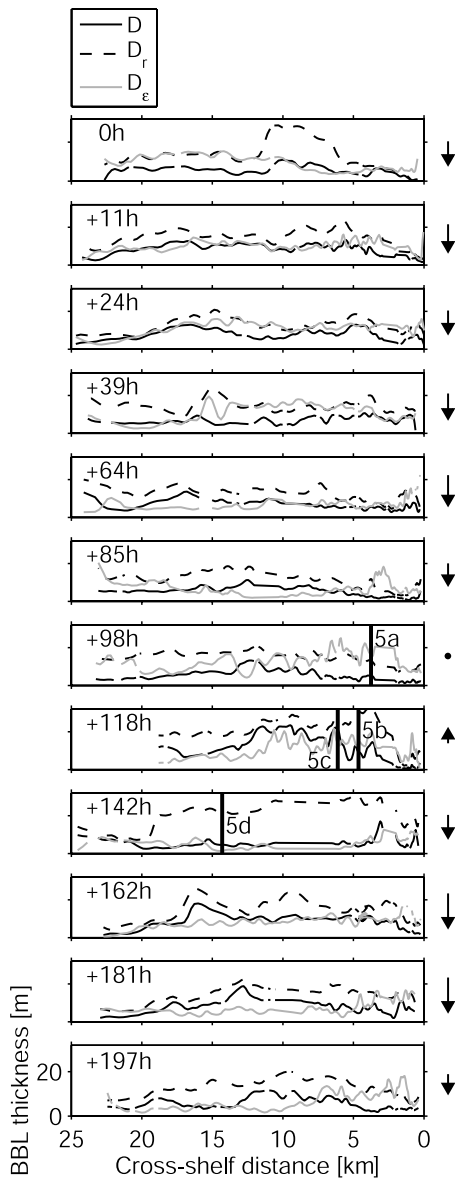


**Figure 6.** Cross-shelf structure and temporal evolution of the BBL. Definitions for each of the layers are given in the text and are demonstrated in Figure 5. Locations of example profiles from Figure 5 are marked on the panels.

Estimates of  $\tau_{yb}$  and  $D_{Ek}$  from near-bottom turbulence measurements are used in section 5.3 to estimate  $u_{Ek}$ .

[23] The above estimate of  $u_{Ek}$  will be compared to the speed at which the location of an isopycnal intersection with the bottom moves across the sloping shelf (we refer to this speed as  $u_b$ ). To begin with, we assume the flow is uniform alongshore ( $\partial\rho/\partial y = 0$ ) and neglect the effects of mixing. In this case, (2) reduces to

$$u_b \frac{\partial\rho}{\partial x} = -\frac{\partial\rho}{\partial t}, \quad (6)$$

from which

$$u_b = -\frac{dx}{dt}. \quad (7)$$

Because  $\partial\rho/\partial x < 0$  (density generally decreases onshore or eastward in the BBL), we write the discretized version

$$u_b = \frac{\Delta x}{\Delta t}, \quad (8)$$

where  $\Delta x$  is the cross-shelf displacement of an isopycnal's intersection with the bottom observed over a time interval  $\Delta t$ . After using this form to compare to our estimate of  $u_{Ek}$ , we address the potential of alongshore heterogeneity and mixing to affect the estimate of  $u_b$ .

## 5.2. $u_b$

[24] The changing cross-shelf location of dense near-bottom fluid is illustrated by highlighting the location of all fluid with  $\sigma_\theta > 26.6$  in individual transects (Figure 8). Upslope movement of near-bottom fluid during upwelling-favorable wind (0–85 hours) was followed by downslope movement as winds eased and reversed (85–142 hours) after which the dense fluid moved back upslope with the resumption of upwelling-favorable winds (142–197 hours).

[25] A measure of the movement of fluid parcels near the bottom is derived from changes in locations of intersections of isopycnals with the bottom. In the event that alongshore variations are of no consequence and vertical mixing is small, these changing locations are due solely to cross-shore motion. For now, we assume this to be the case and revisit the assumption in section 7. Locations of isopycnal bottom intersection ( $\sigma_\theta = 26.65, 26.6, 26.5$ ) for each of the 12 transects is shown in Figure 9. These particular isopycnals were chosen because they represent a relatively large cross-shelf extent (1/3 of the shelf width) and because their bottom intersections can be found in all transects. For the most part, the dense near-bottom fluid appears to maintain its lateral form as it moves across the shelf. The horizontal separation between isopycnals 26.65 and 26.5 is  $\sim 8$  km and this separation does not vary appreciably during the observation period, suggesting that dense near-bottom fluid moves up/down the sloping shelf

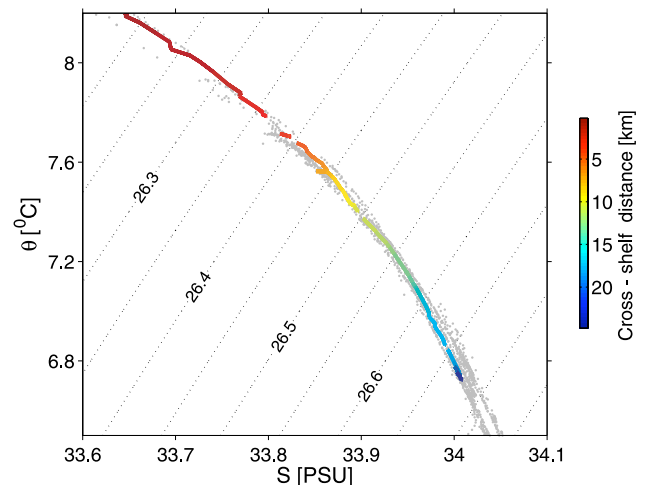


**Figure 7.**  $\theta S$  properties of the fluid lying within the bottom mixed layer. Shaded dots correspond to the data from all 12 transects. The colored line represents the first transect (0 hours) and is coded to represent cross-shelf distance.

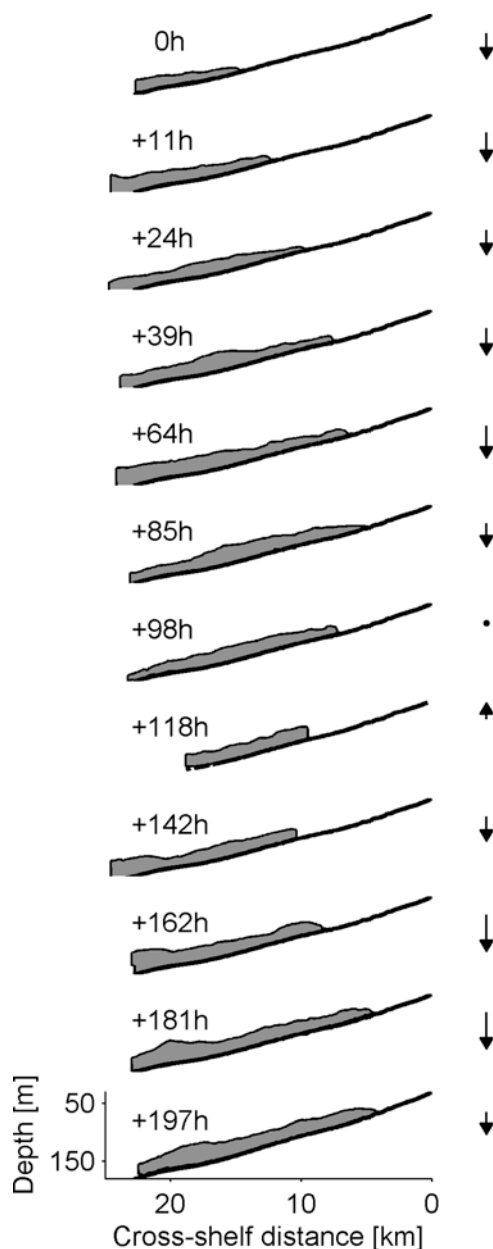


**Figure 8.** Cross-shelf motion of dense near-bottom fluid in response to changes in upwelling conditions. Fluid with  $\sigma_\theta > 26.6$  is shown by shading. The north-south wind stress component averaged over the 24 hour period prior to each transect is shown to the right.

fairly uniformly. A notable exception occurred on 25 May, when the 26.5 isopycnal increased its separation from the others, indicating divergence in the BBL.

[26] The kinematic estimate of the cross-shore near-bottom velocity  $u_b$  is computed from the time rate of change of cross-shelf positions of the isopycnal bottom intersections. This estimate requires the difference in location between successive transects; the time assigned to it is that midway between consecutive measurements of intersections of particular isopycnals with the bottom in consecutive transects. This estimate of  $u_b$  is directly associated with the time-integrated transport of fluid in the BBL. So long as this is

not significantly influenced by shorter timescale fluctuations (i.e., tides),  $u_b$  is an averaged (rather than sampled) speed over the timescale between successive observations. The time histories of  $u_b$  for each of the three isopycnals are shown in Figure 10. Peak speeds are  $6 \text{ km d}^{-1}$  ( $\approx 7 \text{ cm s}^{-1}$ ) eastward following upwelling-favorable winds and almost that fast westward during relaxation and reversal of the winds.

### 5.3. $u_{\text{EK}}$

[27] Determination of  $u_{\text{EK}}$  from (5) requires estimates of both the alongshore component of bottom stress,  $\tau_{yb}$ , and the Ekman layer height,  $D_{\text{EK}}$ . We estimate bottom stress from measurements of  $\varepsilon$  through the BBL. Using a law-of-the-wall formulation, the bottom friction velocity is estimated from which  $\tau_b$  is determined (this method is used and reviewed by *Perlin et al.* [2005a]). Our estimate does not distinguish stress direction, only magnitude. To estimate the component of  $\tau_b$  in the alongshore coordinate direction, we scale it by the ratio of squared alongshore velocity to squared velocity magnitude at height  $D_{\text{EK}}$ ; that is,

$$\tau_{yb} = \tau_b \frac{v_{D_{\text{EK}}}^2}{U_{D_{\text{EK}}}^2}. \quad (9)$$

This scaling indicates  $\tau_b/\tau_{yb} \approx 1.1$  in the region of isopycnal bottom intersection ( $\sigma_\theta = 26.65, 26.6, 26.5$ ). The sign of  $\tau_{yb}$  is determined by the sign of the alongshore velocity at  $D_{\text{EK}}$ . Our estimate of  $D_{\text{EK}}$  is based on the analysis of *Perlin et al.* [2005b], in which several proxies for  $D_{\text{EK}}$  were evaluated. These were compared to the height below which the velocity vector clearly began to veer to the left from above (evaluated from velocity profiles obtained on a mooring near to which we profiled continuously for 50 hours, permitting a comparison of the veering layer estimate to  $D$ ,  $D_r$ , and  $D_\varepsilon$ ), which was taken to be a good measure of  $D_{\text{EK}}$ . From this analysis, it was determined that  $D_\varepsilon$  provided a reasonably good estimate of  $D_{\text{EK}}$  and this was used in evaluating (5). Because the top of the veering layer could not be defined other than from the moored observations, we estimate  $D_{\text{EK}}$  by  $D_\varepsilon$  for the analysis herein.

[28] The temporal variations of  $u_b$  and  $u_{\text{EK}}$  are consistent both in sign and magnitude (Figure 10). The consistency in sign of the two estimates means that the cross-shore motion of isopycnal bottom intersections follows changes in direction of the alongshore velocity atop the BBL. They are also highly correlated (Figure 11).

[29] Since  $\tau_b$  can be written in terms of a friction velocity  $u_*$ , ( $\tau_b = \rho u_*^2$ ) and  $D_{\text{EK}}$  is frequently considered to be a function of  $u_*/f$ , (5) suggests that  $u_{\text{EK}} \propto u_*$ . Further, *Perlin et al.* [2005a] have shown correspondence between  $u_*$  estimated from turbulence profiling measurements and the velocity magnitude 20 m above the bottom estimated from moored velocity measurements. This in turn suggests that  $u_{\text{EK}} \propto U_{20}$  and a reasonable comparison may be obtained from shipboard ADCP measurements that are limited to  $\sim 20$  m above the bottom. As a test, we compare  $u_b$  and the alongshore component of velocity 20 m above the bottom,  $v_{20}$  (Figure 12). The negative correlation is due to the comparison of southward free-stream velocity with eastward Ekman flow. The high correlation suggests the possibility of estimating the cross-shore transport in the bottom

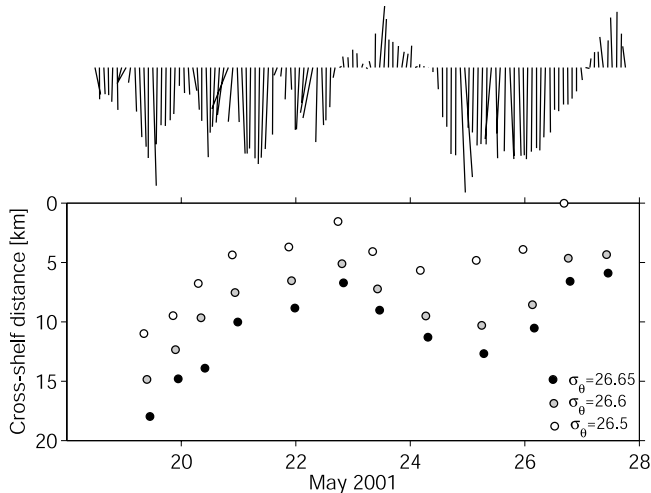


**Figure 9.** Cross-shore location of the intersection where three isopycnals intersect the bottom for all of the 12 transects. At the top of the plot are wind stress vectors.

Ekman layer from shipboard ADCP measurements or moored measurements well above the bottom.

## 6. Bottom Ekman Balance Over a 3 Month Moored Record

[30] An extended test of the Ekman balance (4) in the BBL using moored data requires an indirect estimate of  $\tau_b$ . The result from *Perlin et al.* [2005a],  $u_*^2 = C_D^{20} U_{20}^2$ , is expressed in terms of a drag coefficient evaluated at 20 m height,  $C_D^{20} = 9.8 \times 10^{-4}$ . For comparison, a similar correspondence is evaluated using the observations discussed in this paper. In this case,  $U_{20}$  represents the current speed from shipboard ADCP averaged over 2 km as we transited across the shelf ( $u_*$  is averaged similarly from the turbulence profiles made over the same span of the shelf). The addition of the transect observations to the stationary observations results in  $C_D^{20} = 7.9 \times 10^{-4}$  (Figure 13). (The larger scatter and smaller value of  $C_D^{20}$  from the transect observations may be a consequence of spatial variations in the velocity measured from shipboard ADCP compared to an ADCP measure of velocity at a fixed position.)

[31] The moored velocity observations used to define  $C_D^{20}$  by *Perlin et al.* [2005a] from our 50 hour turbulence profiling time series extended for a period of 3 months from 15 May to 28 August 2001 [*Boyd et al.*, 2002]. Using  $C_D^{20}$ , we compute the Ekman transport in the bottom boundary layer as  $\vartheta_{EK} \tau = C_D^{20} U_{20}^2 / f$ , where  $\tau_b$  has been replaced by  $\rho C_D^{20} U_{20}^2$ . We compare this to

$$\vartheta_{EK} v = \int_0^{D_v} u_{\perp} dz, \quad (10)$$

where  $u_{\perp}(z)$  is the observed velocity perpendicular to that at height  $D_v$ , from a daily-averaged velocity profile filtered to remove currents at tidal periods and shorter. Because  $D_e$  is not available from our moored observations, as it is from our profiling observations,  $D_v$  is used for this particular analysis.  $D_v$  was defined by *Perlin et al.* [2005b] to be the

height at which the veering of the detided velocity toward the bottom begins. For the comparison, we have used the value of  $C_D^{20} = 9.8 \times 10^{-4}$ , determined from coincident and collocated velocity and turbulence measurements. The result (Figure 14) indicates a bottom boundary layer in relative agreement with an Ekman balance over the 3 month duration of the mooring deployment. (For this analysis, two criteria were applied to the daily-averaged velocity profiles: (1) velocity at 8 m height  $\geq 0.05 \text{ m s}^{-1}$  and (2) direction was required to be steady over 2 consecutive days.)

## 7. Discussion

[32] Aside from the contributions of uncertainties in our estimates of  $\tau_b$  and  $D_{EK}$  to the uncertainty in  $u_{EK}$ , there are two terms in the alongshore momentum equation defined by (1) that we have neglected, each of which contribute to the uncertainty in our estimate of  $u_{EK}$ . First, we have neglected local acceleration of the alongshore flow. This term can be estimated from the rate of change of mean alongshore current between consecutive transects. Our analysis indicates that  $1/f(dv/dt)$  is typically 10–30% of the magnitude of  $u_{EK}$ . When added to  $u_{EK}$  in comparison to  $u_b$ , the correlation is marginally improved.

[33] Secondly, we have no measure of the alongshore pressure gradient  $\partial p / \partial y$ . However, results from a regional model described by *Kurapov et al.* [2005] suggest that the

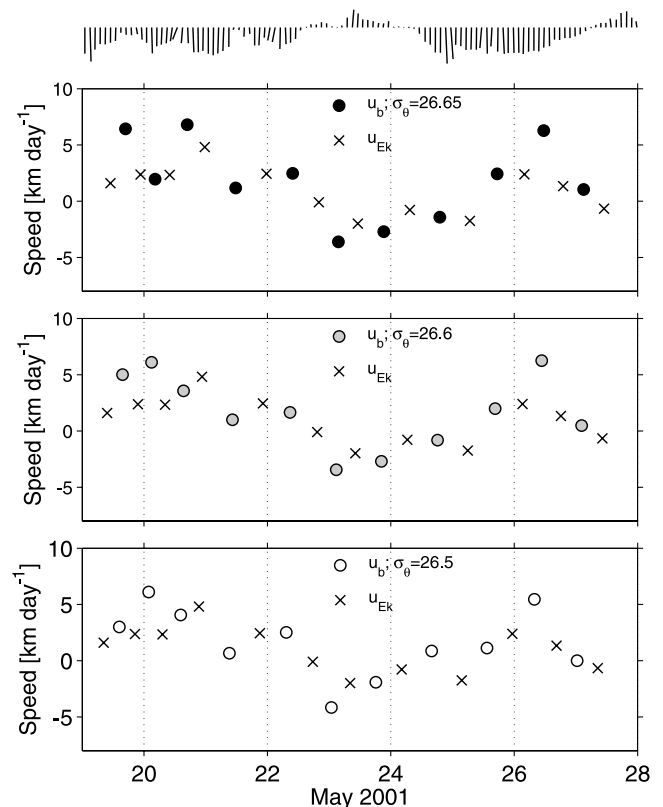


**Figure 10.** Cross-shelf speed of dense near-bottom fluid determined from the rate of change of the intersection of isopycnals corresponding to  $\sigma_{\theta} = 26.5$ , 26.6, and 26.65 with the bottom ( $u_b$ ) and the mean Ekman velocity estimated from bottom stress ( $u_{EK}$ ). Speeds are  $>0$  on-shelf.

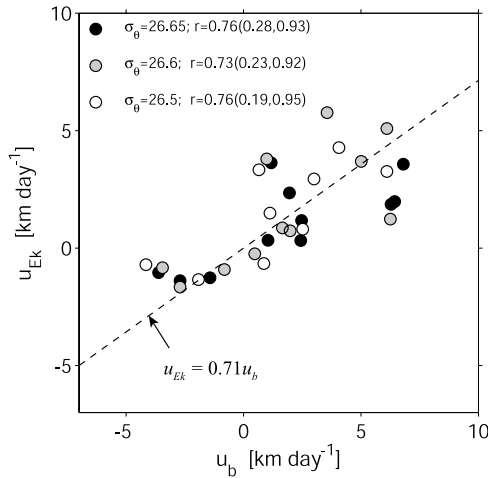


**Figure 11.** Scatterplot of  $u_{EK}$  versus  $u_b$ ;  $r$  is the linear correlation coefficient, and 95% confidence intervals for neutral regression and correlation coefficients are shown in parentheses. A neutral regression is used because neither parameter is independent [Emery and Thomson, 2001, p. 247].

magnitude of this term is similar to that of the alongshore acceleration term during our observation period. In vertically integrating (3) to arrive at (4), we have stated that the stress at  $D_{EK}$  is small. In fact, by definition of  $D_{EK}$ , it has to be small or 0. The rationale is that turbulence generated by interaction with the bottom diminishes away from it. However, externally generated turbulence in the interior away from the bottom may result in turbulent stress at  $D_{EK}$ . When and where this occurs, the integration limit at  $D_{EK}$  may be significant and the balance in the Ekman layer modified by turbulence external to it. We have estimated the turbulent stress following the method of Dillon *et al.* [1989] and it seems that occurrences of high stress at  $D_{EK}$  exist but are rare in our observations. The local implications of the exceptions are a topic for further study. Our estimate of  $u_b$  represents a simplification of (2). We have no measure of alongshore density gradient. While there were accompanying measurements from a second ship at the time of our observations, these did not include measurements sufficiently deep to include the near-bottom fluid of interest here. In general, though, we expect the alongshore gradients in density to be much less than cross-shore gradients, smaller than the ratio of cross-shore to alongshore currents near the bottom, so that alongshore advection of density is small compared to cross-shore advection in (2). This appears to be the case based on the results from a modeling study of near-bottom flow in this region [Oke *et al.*, 2002].

[34] There is considerable cross-shelf structure in the density of the fluid within the BBL (Figure 15). There are several instances of cross-shelf discontinuities in density. This suggests a richness in the structure of the cross-shelf flow that will be quite difficult to observe in detail. It is possible (though difficult to test with the available data) that cross-shelf divergence in the bottom Ekman transport can result in such a structure. This, of course, directly implies three-dimensionality of the motion in the BBL that we are unable to resolve with these observations.

[35] In setting  $\partial J_b / \partial z$  to 0 in (2), we have neglected the influence of mixing. However, turbulent mixing modifies the position of isopycnals (both vertically and horizontally) and hence the locations at which they intersect the bottom. In stably stratified fluid, mixing will always cause near-bottom fluid to become less dense. Over a sloping bottom, this will result in the location of an isopycnal bottom intersection to move downslope. To isolate this effect we assume there is no advection and local change of density is due solely to turbulent buoyancy flux. This change in density would contribute an “apparent” advective term,

$$u_i \frac{\partial \rho}{\partial x} = \frac{\rho_0}{g} \frac{\partial J_b}{\partial z}, \quad (11)$$

integrated over the mixed layer height:

$$\int_0^D u_i \frac{\partial \rho}{\partial x} dz = \frac{\rho_0}{g} J_b(z = D). \quad (12)$$

Since isopycnals are vertical in the mixed layer, neither  $u_i$  nor  $\partial \rho / \partial x$  is a function of  $z$ :

$$u_i \frac{\partial \rho}{\partial x} D = \frac{\rho_0}{g} J_b(z = D). \quad (13)$$

The velocity  $u_i$  represents the cross-shelf speed of the location of an isopycnal’s bottom intersection due solely to vertical mixing. It must always be directed offshore. We can evaluate the turbulent diffusivity,  $K_\rho$ , from our turbulence profiling measurement [Osborn, 1980] as

$$K_\rho = \frac{\Gamma \varepsilon}{N^2}, \quad (14)$$

where  $\Gamma$  is a mixing efficiency taken to be 0.2 [Moum, 1996; Smyth *et al.*, 2001]. Our discrete estimates of  $u_i$  indicate it to be relatively small, infrequently exceeding

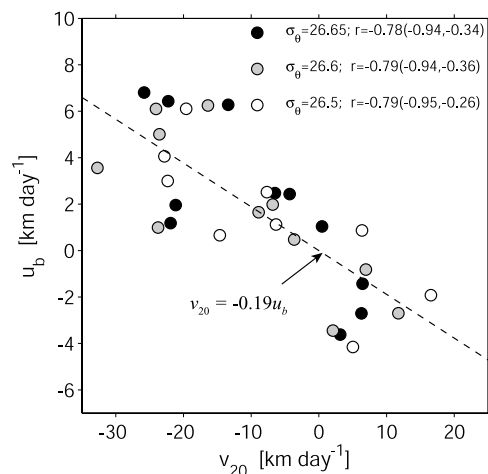


**Figure 12.** Scatterplot of alongshore velocity 20 m above the bottom ( $v_{20}$ ) versus  $u_b$ ;  $r$  is the linear correlation coefficient, and 95% confidence intervals for regression and correlation coefficients are shown in parentheses.

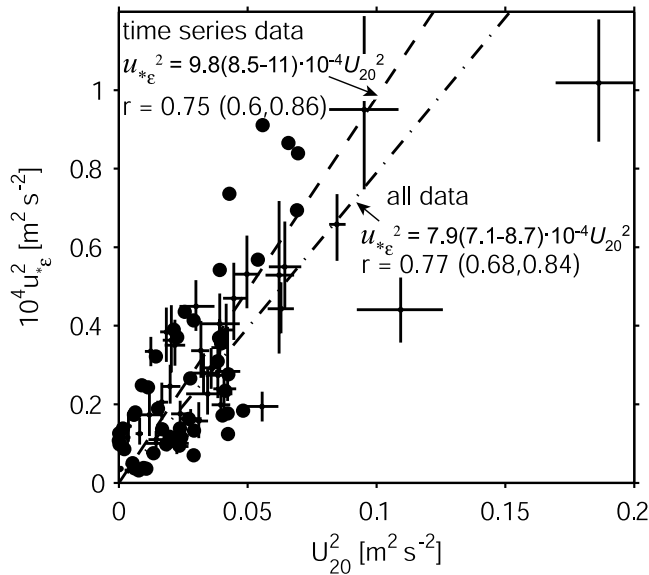


**Figure 13.** Comparison of squared friction velocity to squared current speed at 20 m height. Black circles show 1 hour averaged time series data, and crosses (the length of which indicates 95% confidence limits of estimates) show 2-km-averaged data from cross-shore transects. Variable  $r$  is the linear regression coefficient, and 95% confidence intervals for regression and correlation coefficients are shown in parentheses.

$0.2 \text{ km d}^{-1}$ . Tidal motion also contributes to cross-shore motion of near-bottom fluid. While barotropic tidal motions are small, baroclinic tidal velocities peaked at  $0.08 \text{ m s}^{-1}$  during our observation period (from a midshelf mooring in 81 m water depth [Boyd *et al.*, 2002]). Even though we alias the tides in our transect observations, the resultant tidal excursion of less than 0.5 km has little effect on our estimate of  $u_b$ .

[36] Other than the effect of mixing on  $u_b$ , all other effects are random and hence we expect they will result in

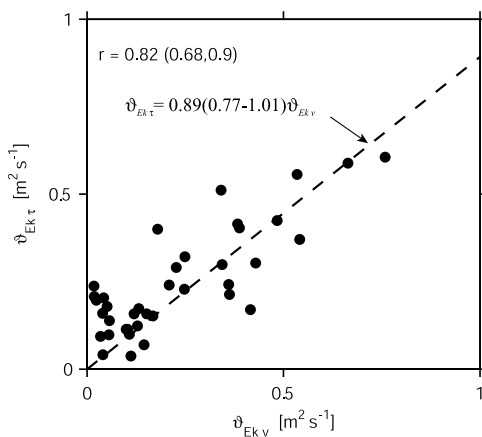


**Figure 14.** Comparison of the transport computed by vertical integration of the velocity perpendicular to that at height  $D_{EK}$  using moored velocity data (3 month time series), and the Ekman transport computed from bottom stress using a drag coefficient and the current speed at 20 m.

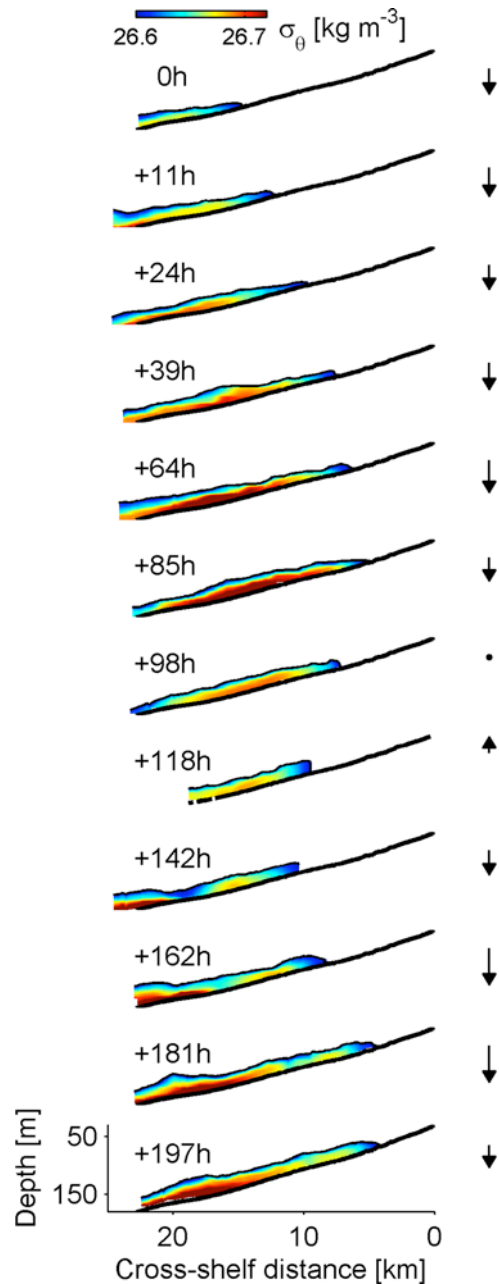


**Figure 15.** Reproduction of Figure 8 with the density of the fluid ( $\sigma_\theta > 26.6$ ) within the BBL image-colored to indicate the variability there.

increased scatter of the comparison shown in Figure 11.  $u_{EK}$  represents an averaged value of the cross-axis velocity over the Ekman layer defined by  $D_{EK}$ . However, because the flow both veers toward the bottom and decreases in magnitude to satisfy the bottom boundary condition, the cross-axis velocity is not constant over  $D_{EK}$ . In fact, the cross-axis velocity has a maximum value in the lower 10–15 % of the Ekman layer [see Perlin *et al.*, 2005b], below which it must rapidly  $\rightarrow 0$ . In contrast,  $u_b$  represents an estimate of the flow speed averaged over  $D$ . Where  $D = D_{EK}$ , these two estimates represent equivalent vertical averages. Where they differ, the averaging is biased. For the most part,  $D$  and  $D_{EK}$  are not substantially

different (Figure 6) and this effect is not likely to be significant.

## 8. Summary

[37] By repeating transects of currents, density, and turbulence through the BBL across a relatively uniform stretch of the continental shelf off Oregon, we have been able to observe the response of the BBL to variations in winds and currents in some detail. We had the good fortune to make these observations coincident with a sequence of strong upwelling-favorable winds followed by relaxation and subsequent resumption of upwelling.

[38] By all measures, the thickness of the BBL is greatest and turbulence there is most intense during the relaxation from upwelling. This is consistent with the observations of *Trowbridge and Lentz* [1991]. From a subset of the observations described here, *Moum et al.* [2004] have suggested how convectively driven mixing can be responsible for both the intense mixing and thickened boundary layer as light near-bottom fluid is drawn beneath denser fluid during downslope flow. Upon the resumption of upwelling-favorable winds, and when the downslope motion ceases, turbulence dies in the absence of other sources (low current velocities in the interior and therefore low levels of shear-generated turbulence near the bottom). The well-mixed bottom layer thins, leaving a thick remnant layer with low stratification. Advection of dense near-bottom fluid upslope by Ekman transport during upwelling increases the density difference between the boundary layer and the interior, so that vertical transport near the top of the layer is suppressed, and the growth of the BBL is inhibited.

[39] By tracking the intersection of near-bottom isopycnals with the bottom over successive transects, we estimate the cross-shore speed of near-bottom fluid  $u_b$ . This estimate is based on the transport of fluid with specific density. It correlates well and is approximately equal to a dynamic estimate of mean Ekman velocity. This test suggests that the Ekman balance holds across a significant cross-shore extent of the continental shelf, not only at a particular location [*Trowbridge and Lentz*, 1998]. By extending this calculation to a 3 month record of moored velocities, we verify the Ekman balance in the BBL over the period 15 May to 28 August 2001, at a midshelf location on the Oregon coast.

[40] **Acknowledgments.** This work was funded by the National Science Foundation. Mike Neeley-Brown, Ray Kreth, Greig Thompson, and Gunnar Gunderson helped to obtain these data. The moored velocity data was kindly provided by Tim Boyd, Mike Kosro, and Murray Levine. The captain and crew of the R/V *T. G. Thompson* were helpful in all regards.

## References

- Boyd, T., M. D. Levine, P. M. Kosro, S. R. Gard, and W. Waldorf (2002), Observations from moorings on the Oregon continental shelf, May–August 2001, *Data Rep. 190 2002-6*, Oregon State Univ., Corvallis.
- Dickey, T. D., and J. C. van Leer (1984), Observations and simulations of bottom Ekman layer on a continental shelf, *J. Geophys. Res.*, *89*, 1983–1988.
- Dillon, T. M., J. N. Moum, T. K. Chereskin, and D. R. Caldwell (1989), Zonal momentum balance at the equator, *J. Phys. Oceanogr.*, *19*, 561–570.
- Emery, W. J., and R. E. Thomson (2001), *Data Analysis Methods in Physical Oceanography*, 2nd ed., 638 pp., Elsevier, New York.
- Kundu, P. K. (1976), Ekman veering observed near the ocean bottom, *J. Phys. Oceanogr.*, *6*, 238–242.
- Kurapov, A. L., J. S. Allen, G. Egbert, R. Miller, P. M. Kosro, M. D. Levine, T. Boyd, J. A. Barth, and J. N. Moum (2005), Assimilation of moored velocity data in a model of coastal wind-driven circulation off Oregon: Multivariate capabilities, *J. Geophys. Res.*, doi:10.1029/2004JC002493, in press.
- Lass, H. U., and V. Mohrholz (2003), On dynamics and mixing of inflowing saltwater in the Arkona Sea, *J. Geophys. Res.*, *108*(C2), 3042, doi:10.1029/2002JC001465.
- Lentz, S. J., and J. H. Trowbridge (1991), The bottom boundary layer over the northern California shelf, *J. Phys. Oceanogr.*, *21*, 1186–1201.
- Mercado, A., and J. van Leer (1976), Near bottom velocity and temperature profiles observed by cyclosonde, *Geophys. Res. Lett.*, *3*, 633–636.
- Moum, J. N. (1996), Efficiency of mixing in the main thermocline, *J. Geophys. Res.*, *101*, 12,057–12,069.
- Moum, J. N., M. C. Gregg, R. C. Lien, and M. E. Carr (1995), Comparison of turbulence kinetic energy dissipation rate estimates from two ocean microstructure profilers, *J. Atmos. Oceanic Technol.*, *12*, 346–366.
- Moum, J. N., A. Perlin, J. M. Klymak, M. D. Levine, T. Boyd, and P. M. Kosro (2004), Convectively-driven mixing in the bottom boundary layer over the continental shelf during downwelling, *J. Phys. Oceanogr.*, *34*, 2189–2202.
- Oke, P. R., J. S. Allen, R. N. Miller, and G. D. Egbert (2002), A modeling study of the three-dimensional continental shelf circulation off Oregon. Part II: Dynamical analysis, *J. Phys. Oceanogr.*, *32*, 1383–1403.
- Osborn, T. R. (1980), Estimates of the local rate of vertical diffusion from dissipation measurements, *J. Phys. Oceanogr.*, *10*, 83–89.
- Pedlosky, J. (1987), *Geophysical Fluid Dynamics*, 2nd ed., 710 pp., Springer, New York.
- Perlin, A., J. N. Moum, J. M. Klymak, M. D. Levine, T. Boyd, and P. M. Kosro (2005a), A modified law-of-the-wall applied to oceanic bottom boundary layers, *J. Geophys. Res.*, doi:10.1029/2004JC002310, in press.
- Perlin, A., J. N. Moum, J. M. Klymak, M. D. Levine, T. Boyd, and P. M. Kosro (2005b), Concentration of Ekman transport in the bottom boundary layer by stratification, *J. Geophys. Res.*, doi:10.1029/2004JC002641, in press.
- Saylor, J. H. (1994), Studies of bottom Ekman layer processes and mid-lake upwelling in the Laurentian Great Lakes, *Water Pollut. Res. J. Can.*, *29*, 233–246.
- Saylor, J. H., and G. M. Miller (1988), Observation of Ekman veering at the bottom of Lake Michigan, *J. Great Lakes Res.*, *14*, 94–100.
- Smyth, W. D., J. N. Moum, and D. R. Caldwell (2001), The efficiency of mixing in turbulent patches: Inferences from direct simulations and microstructure observations, *J. Phys. Oceanogr.*, *31*, 1969–1992.
- Trowbridge, J. H., and S. J. Lentz (1991), Asymmetric behavior of an oceanic boundary layer above a sloping bottom, *J. Phys. Oceanogr.*, *21*, 1171–1185.
- Trowbridge, J. H., and S. J. Lentz (1998), Dynamics of the bottom boundary layer on the northern California shelf, *J. Phys. Oceanogr.*, *28*, 2075–2093.
- Weatherly, G. L. (1972), A study of the bottom boundary layer of the Florida current, *J. Phys. Oceanogr.*, *2*, 54–72.

J. M. Klymak, Scripps Institution of Oceanography, University of California, San Diego, 9500 Gilman Drive, La Jolla, CA 92093-0213, USA. (jklymak@ucsd.edu)

J. N. Moum and A. Perlin, College of Oceanic and Atmospheric Sciences, 104 Ocean Admin Building, Oregon State University, Corvallis, OR 97331-5503, USA. (moum@coas.oregonstate.edu; aperlin@coas.oregonstate.edu)